Heliyon 9 (2023) e20333

Contents lists available at ScienceDirect

Heliyon

journal homepage: www.cell.com/heliyon

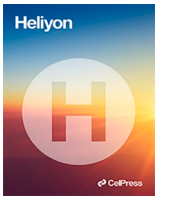

Performance enhancement and optimization of residential air conditioning system in response to the novel FAl_2O_3-POE nanolubricant adoption

A. Nugroho [a,b,*], R. Mamat [a,b], J. Xiaoxia [a], Z. Bo [a], M.F. Jamlos [c], M.F. Ghazali [d]

[a] School of Mechanical Engineering, Ningxia University, 750021, China
[b] Centre for Automotive Engineering, Universiti Malaysia Pahang, 26600, Malaysia
[c] Faculty of Electrical & Electronics Engineering Technology, Universiti Malaysia Pahang, Malaysia
[d] Centre for Research in Advanced Fluid and Processes, University Malaysia Pahang, Malaysia

ARTICLE INFO

Keywords:
Functionalized Al_2O_3
FAl_2O_3–POE nanolubricant
Air conditioning systems
Central composite design optimization
Response surface methodology (RSM)

ABSTRACT

This paper aims to evaluate residential air conditioning systems' performance enhancement and optimization by adopting a novel functionalized Al_2O_3 (FAl_2O_3)–Polyolester (POE) nanolubricant. Comprehensive discussions were conducted on key performance parameters, including heat absorption, compressor work, cooling capacity, coefficient of performance (COP), and power consumption. Novel FAl_2O_3 nanoparticles were dispersed into the POE lubricant using a two-step method. The findings reveal that FAl_2O_3–POE nanolubricant exhibits superior heat absorption compared to pure POE. Heat absorption decreases with an increased initial refrigerant charge, while cooling capacity performance improves with an increased initial refrigerant charge. The COP shows an increasing trend at all concentrations of FAl_2O_3–POE nanolubricant when operating with R32. FAl_2O_3–POE/R32 demonstrates an enhanced range of 3.12%–32.26% for COP. The results suggest that applying novel FAl_2O_3–POE nanolubricant with R32 can reduce electrical power consumption by 13.79%–19.35%. The central composite design (CCD) offers an optimal condition for FAl_2O_3–POE nanolubricant with a concentration of 0.11 vol%, an initial refrigerant charge of 0.442 kg, resulting in a COP of 3.982, a standard error of 0.019, and a desirability of 1.0.

1. Introduction

Air conditioning technology plays an essential role in modern life [1]. However, refrigerants with high Global Warming Potential (GWP) have a more significant heating effect on the surrounding air, resulting in lower energy efficiency. Increasing the use of air conditioning systems that utilize high GWP refrigerants will lead to amplified global warming effects and higher energy consumption [2]. Montreal Protocol requires that the refrigerant air conditioning system have zero ozone depletion potential (ODP) and lower GWP [3]. R410a has been adopted as a refrigerant in residential air conditioning systems because it possesses zero ODP and a GWP of 2088 [4]. Therefore, there is a need for an alternative refrigerant that possesses zero Ozone Depletion Potential (ODP) and lower Global Warming Potential (GWP) as a replacement for the current refrigerant R410a. Such a replacement would effectively mitigate the global warming effect and contribute to energy sector sustainability by reducing energy consumption [5].

* Corresponding author. School of Mechanical Engineering, Ningxia University, 750021, China.
E-mail address: ir.agusnug@gmail.com (A. Nugroho).

https://doi.org/10.1016/j.heliyon.2023.e20333
Received 1 July 2023; Received in revised form 15 September 2023; Accepted 19 September 2023
Available online 26 September 2023

In recent years, nanolubricants have emerged as a promising solution for improving the performance of air conditioning systems. Nanoparticles, such as Functionalize Al2O3 (FAl2O3) nanoparticles, have demonstrated exceptional properties that can enhance the base fluid's thermal conductivity and lubrication characteristics [6–8]. Incorporating these nanoparticles into the lubricant matrix offers the potential to optimize heat transfer, reduce friction losses, and improve overall system efficiency [9]. Moreover, nanolubricants have shown the ability to mitigate wear and tear on system components, leading to an extended equipment lifespan and reduced maintenance requirements [10].

Several studies have investigated the application of nanolubricants in air conditioning systems, focusing on their impact on key performance parameters. The addition of nanoparticles has enhanced heat absorption capabilities, improving cooling efficiency [11]. Furthermore, nanolubricants have shown promise in reducing compressor work, resulting in energy savings and increased system reliability [12]. These findings highlight the potential of nanolubricants to contribute to the development of sustainable and energy-efficient air conditioning technologies [13].

Furthermore, Sanukrishna et al. [14] reported that the thermal conductivity of nanolubricant could be increased by 1.38% at 0.8 vol% by dispersing TiO2 in PAG. Xu et al. stated that replacing R410a with R32 resulted in a 2–9% improvement in overall performance. As reported by Xu et al., the increase in discharge compressor temperature promotes a loss in compressor efficiency, which results in a decrease in the air conditioning system's coefficient of performance [15]. Panato et al. [16] observed that replacing R410a with R32 decreased overall performance between 4 and 14% in the following evaporator temperature range −5 to 5 °C. Thus, many previous researchers have made significant efforts into improving refrigeration system performance by adopting nanolubricants. COP can be enhanced by 37.3 at 0.5 vol% by adopting MWCNT/POE in the air conditioning system, as reported by Salem et al. [17].

Pico et al. [18] reported that adopting Diamond/POE for the RAC system enhanced COP by 4 and 8% at 0.1 and 0.5 vol%. COP of the RAC system could be increased by 2.06% by adopting TiO2–MO, as reported by Jatinder et al. [19]. A recent finding from Nawaf et al. [20] reported dispersing nanodiamond at 0.05–0.5 vol% in polyolester. According to tribology assessment results, nanolubricant with a concentration of 0.1 vol% has the lowest coefficient of friction (COF) compared to others. Recently, Ahmed et al. [21] formulated a TiO2–mineral oil nanolubricant that works with R32 and R22 (75:25%) labelled as mixture 1 and R32 and R600a (75:25%) labelled as mixture 2. The results reveal that pure R32 has the same compressor work as R22, but a mixture of 1 and 2 can lower compressor work by 33% when TiO2–MO nanolubricant with 0.02 vol% is used. Chauhan [22] claimed that he synthesized Al2O3–SiO2/Polyalkylene Glycol (PAG46) at various volume concentrations ranging from 0.02% to 0.1% and examined it with the refrigerant R134a. According to the experimental results, an Al2O3–SiO2 nanolubricant concentration of 0.08 vol% is an optimum concentration since it lowered compressor power by up to 10.89% compared to pure PAG lubricant. Evidence suggests that Al2O3–SiO2/PAG46 with 0.08 vol% concentration is ideal for automobile air conditioning systems.

Upon a thorough review of the existing literature, it is evident that there is a need for more studies investigating the direct application of nanolubricants in air conditioning systems across diverse operating conditions. Furthermore, it is essential to acknowledge the necessity of creating a universal nanolubricant solution applicable to all air conditioning systems. Therefore, this manuscript addresses these gaps by presenting a comprehensive evaluation of the refrigerant effect, compressor work, overall performance, and cooling capacity of residential air conditioning systems upon adopting a novel FAl2O3–POE nanolubricant.

The main objective of this study is to address the challenge of enhancing performance in the context of refrigerant R32 when compared to the existing refrigerant R410a. By investigating the utilization of the FAl2O3–POE nanolubricant, this research presents a potential solution for enhancing the overall system performance. A systematic approach based on the central composite design of the response surface methodology is employed to determine the optimal nanolubricant configuration that effectively operates in conjunction with refrigerant R32 to achieve this goal.

2. Experimental procedure

2.1. Materials

The aluminum oxide nanoparticles used in this research were obtained from Sigma-Aldrich in Saint Louis, Missouri, USA. Alumina was selected for its performance characteristics, including heat conductivity, density, and shape. Alumina, being naturally polar nanoparticles, presents challenges in dispersing within predominantly non-polar synthetic oils. Consequently, Al_2O_3 functionalization treatment is necessary to modify the surface of Al_2O_3 nanoparticles. This process is detailed in the following sub-section. SUNISO from Belgium supplied the polyolester (POE) lubricant, a synthetic refrigerant oil. Tables 1 and 2 present the fundamental properties of Al_2O_3 and Polyolester (POE), respectively.

Table 1
Al2O3 physical nanoparticles properties [23].

Properties	Metric
Density	3.95 g/cm^3
Molar mass	101.96 g/mol
Diameter	13 nm
Color	White
Melting point	2040 °C
Boiling Point	2977 °C

2.2. Functionalization of Al2O3 nanoparticle and characterization method

The goal of the functionalization process is to transform the polar Al2O3 surface into a non-polar one. The Al2O3 functionalization process incorporates non-polar SiO2 nanoparticles and ethanol, serving as the modifier material and solvent, respectively. SiO2 nanoparticles are chosen as the modifier material due to their predominant non-polar properties arising from silica. Yuan et al. [25] reported that the functionalization process was carried out by silica adsorption to the alumina. Ethanol (C2H6O) was chosen as the solvent agent in this process because the non-polar ethyl (C2H5) group molecules could enhance the wettability effect of SiO2 on Al2O3 surfaces [26]. Thus, the Al2O3 and SiO2 dispersion in ethanol can increase SiO2 adsorption on Al2O3 and formulate non-polar FAl2O3. After formulating the FAl2O3 nanolubricant, the nanoparticles were mixed into the POE lubricant to create the nanolubricant [27]. The schematic diagram of the functionalization process is shown in Fig. 1. The FAl2O3 nanoparticles were subsequently characterized using Transmission Electron Microscopy (TEM) FEI Tecnai G2 T20 X-TWIN to assess their morphology and diameter size. The dimensions of FAl2O3 were further confirmed using Image J software. The energy dispersive X-ray spectroscopy (EDX) method was adopted to assess the newly synthesized FAl2O3 nanoparticles' elements.

2.3. Nanolubricants preparation and visual observation method

The nanolubricant in this study was formulated using a two-step method. he two-step method involves two primary stages for formulating the nanolubricant: first, mixing the nanoparticle dispersion into the lubricant to create the nanolubricant, and second, applying ultrasonication treatment. This two-step method involves four stages that must be performed in a specific sequence [28]. The initial stage involves weighing the required nanoparticles and POE lubricant for the dispersion process based on volume concentration. The volume of nanolubricant concentration is determined using Equation (1), as suggested by Azmi et al. [29]. The nanolubricant preparation process flow is depicted in Fig. 2.

The second stage involves dispersing nanoparticles into the POE lubricant using a magnetic stirrer for 30 min without applying heat. The magnetic stirrer used in this study is the FAVORIT Stirring Hotplate HS0707V2. In the third stage, ultrasonic treatment is applied to the nanolubricant for 100 min to enhance its stability and prevent agglomeration. Ultrasonication treatment was conducted in three cycles of 40-40-20 min for each sample, with a 15-min pause in between to prevent a significant temperature increase in the nanolubricant and ensure compliance with device safety standards [30]. An ultrasonic homogenizer with a probe was chosen for its ability to provide stronger vibrations to the suspension, resulting in better dispersion compared to using an ultrasonic bath, as reported by Mellado et al. [31]. The ultrasonic homogenizer used in this study is the Hielscher Ultrasonics Germany UP400S.

Formulating the FAl2O3-POE nanolubricant required three phases. The initial phase involved Al2O3 nanoparticles and POE lubricant measurement. Nanoparticles were weighed using the digital weighing scale Sartorius Entris to determine the necessary mass of Al2O3 nanoparticles and POE lubricant before mixing. Beforehand, the balance was calibrated to achieve a suitable level and fine-tune the validation of the circle center's leveling bubble. The middle stage encompassed mixing the base lubricant (POE lubricant) and Al2O3 nanoparticles using a magnetic stirrer for 30 min. The third stage involved the ultrasonication process using an ultrasonic homogenizer. Interlude mode was employed to disperse the nanolubricant agglomeration for 100 min. Equation (1), as suggested by Sharif et al. [32], was utilized to estimate the volume fraction of the nanolubricants. After each 40-min cycle, a 15-min interlude was applied to prevent deterioration of nanolubricant homogeneity [33].

$$\varnothing = \frac{m_p/\rho_p}{m_p/\rho_p + m_l/\rho_l} \, x \, 100\% \tag{1}$$

Here, ∅ represents the nanoparticle volume concentration in %; mp and ml stand for the masses of the nanoparticle and POE lubricant, respectively, while ρn and ρl denote the density of the Al2O3 nanoparticle and POE lubricant, respectively. The prepared FAl2O3-POE nanolubricants were stored in experimental tubes to assess their stability through observation of aggregation and sedimentation.

2.4. Experimental facility and procedure

To conduct the experimental procedure, we constructed an in-house developed calorimeter to assess the performance of the RAC system. The RAC system installed in the experiment chamber has a capacity of one horsepower. The layout and design of the experiment chamber, referred to as the calorimeter chamber, are shown in Fig. 3. The RAC system is designed in a back-to-back configuration, wherein the interior and outdoor units are positioned opposite each other, following the suggestion of previous researchers [34–36]. The RAC system is installed in a room equipped with a calorimeter for control [36]. Fig. 3 was designed to replicate

Table 2
Properties of Polyolester oil [24].

Lubricant	Properties					
	Viscosity at 40 °C	Viscosity at 100 °C	Viscosity Index	Density At 15 °C	Flash Point	Pour Point
Suniso SL 68	70.1 cSt	9.1 cSt	105	0.960 g/cm^3	252 °C	−36 °C

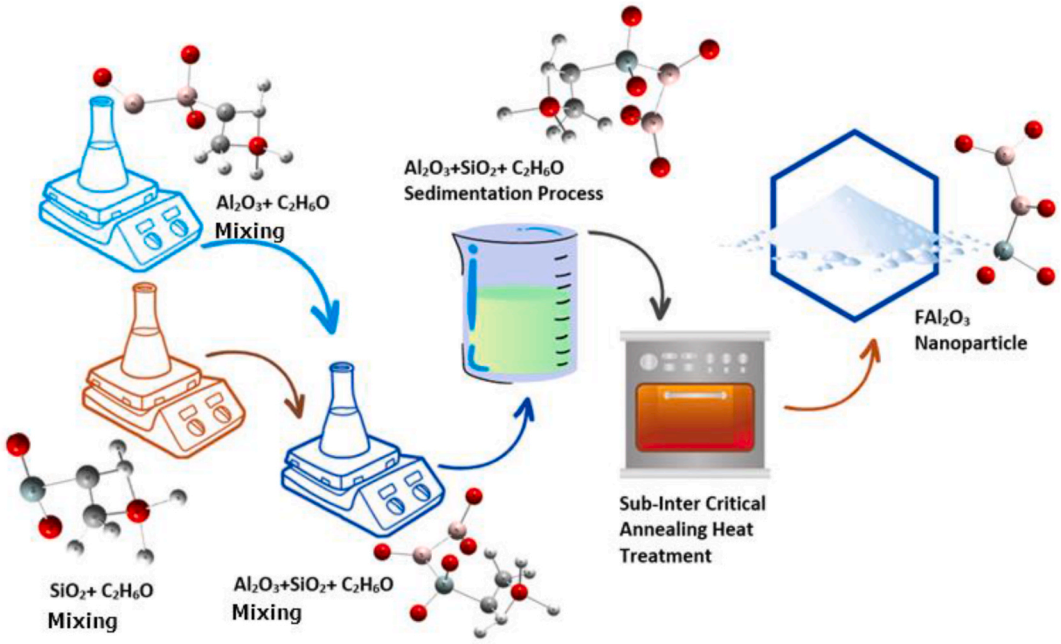

Fig. 1. Process flow of Al_2O_3 functionalization

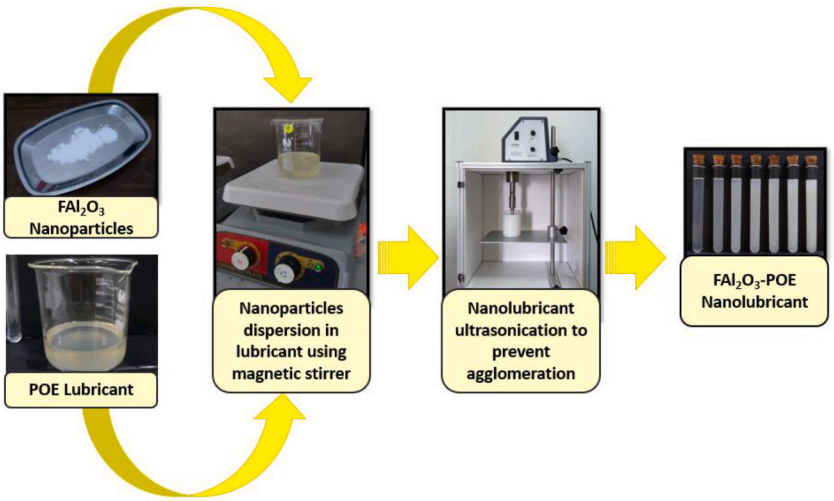

Fig. 2. FAl_2O_3-POE nanolubricant formulation using the two-step method.

real-world conditions and tailored to meet the needs of the experimental study. Its construction guarantees a controlled environment, facilitating effective conduct of our experiments. The core aim of the distinct chamber, illustrated in Fig. 3, is to proficiently regulate indoor and outdoor temperatures and humidity levels, aligning with the testing criteria outlined in Table 3. This controlled setting guarantees that the experimental conditions closely adhere to the standard's guidelines. Through the implementation of the separate chamber, we can effectively simulate real-world conditions while exercising essential control over variables. This facilitates precise and reliable measurements of the air conditioning system's performance.

A 2-inch square iron structure supports the frame of the calorimeter chamber, while the design of the members employs 1-inch square iron. Exterior walls are constructed from 2 mm plywood, while interior walls are composed of 2-inch polystyrene to inhibit heat transfer between the surrounding air and the controlled chamber, as suggested by previous researchers [38,39]. Silicone rubber is applied to seal the spaces between the polystyrene joints, preventing any leakage of heat transfer.

The key components of the calorimeter include 1. indoor unit, 2. outdoor unit, 3. equipment under test, 4. heating unit, 5. humidifier unit, 6. fan, 7. mixer, 8. air sampling tube, 9. pressure equalization device, and 10. exchange air fan. For the air conditioning system setup, no modifications were applied to the specifications. This is because all component specifications used in the setup align

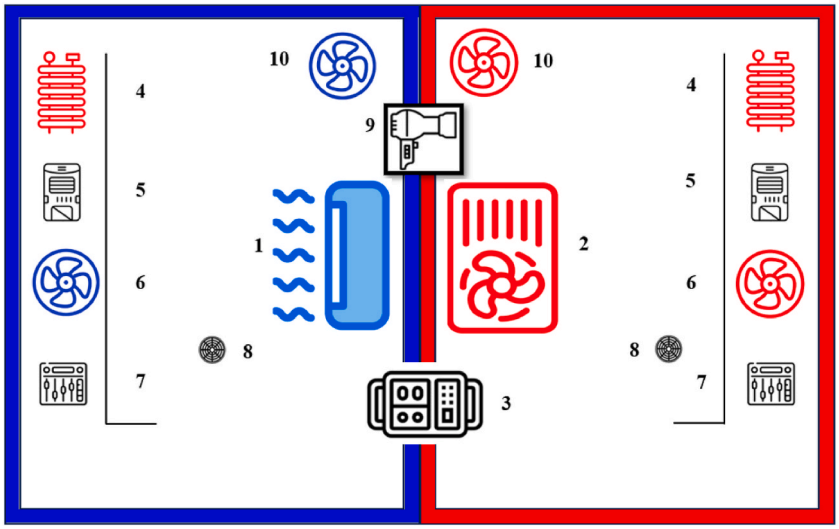

Fig. 3. Calorimeter RAC experiment layout.

Table 3
Performance test conditions [37].

Parameter	Standard Rating Condition		
	T_1	T_2	T_3
Dry bulb temperature in indoor side	32 °C	27 °C	32 °C
Dry bulb temperature in outdoor side	43 °C	35 °C	52 °C

with the standard specifications provided by the manufacturer. This approach is adopted to ensure optimal performance, in line with the factory-defined requirements indicated on the air conditioning system's nameplate. This is consistent with the suggestion of previous researchers [40–42].

The performance test in this study was conducted under T1 conditions in a moderate climate. All tests were carried out with the equipment operating under full-load conditions. In order to establish a moderate climate, a 900 W electric heater was placed inside the indoor room. Fig. 4 illustrates the performance test of the RAC system using POE nanolubricants in the context of R410a and R32 system flow.

A 1 HP rotary compressor was utilized in the setup of the RAC system. Pure POE lubricant is introduced into the RAC system at the

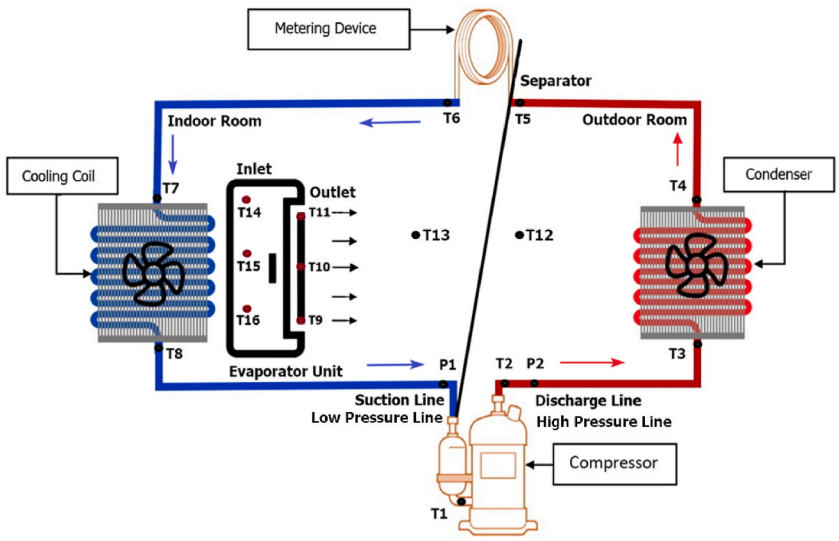

Fig. 4. The schematic diagram illustrates the setup of the RAC system, depicting the positions of the thermocouples.

commencement of each assessment for the next concentration. This is done to prevent any contamination from the previous nano-lubricant to the succeeding one [11]. This process is repeated three times for the FAl2O3-POE nanolubricant.

Sixteen K-type thermocouples were positioned as indicated in Table 3 to record and quantify temperatures during the test. K-type thermocouples were installed using snug, non-conductive insulation material to prevent temperature transfer between the sensor and the surrounding environment, as advised by previous researchers [43,44]. Throughout the test, the RAC system settings were configured for full-speed fan conditions, and the barometric pressure location remained constant. Grille and damper positions, as well as fan speed, were adjusted to full speed according to the manufacturer's instructions, and no changes were made to these settings in accordance with the standard as suggested by Zhou et al. [36].

The RAC system performance test refers to the maximum cooling performance within the T1 setting, specifically denoted as the standard cooling rating for a moderate climate [45]. The schematic diagram in Fig. 4 illustrates the position of each thermocouple within the RAC system setup. The performance test conditions at T1 were as follows: the indoor and outdoor temperatures were maintained at 32 °C and 43 °C, respectively, both during conditioning and RAC system testing. Consequently, a 900-Watt electric heater fan is installed and activated, providing consistent heating during the conditioning and testing phases to uphold a stable indoor temperature of 32 °C.

The RAC system within the calorimeter is initially operated until it achieves a steady-state (equilibrium) condition, preventing data fluctuations; the difference in the steady state should not exceed 0.3%. Preparation for the steady-state condition was upheld for a minimum of 1 h before recording performance test data. To meet the consistency and accuracy standards of data, continuous data recording for at least 30 min without interruption was mandated by performance testing requirements, in alignment with the standard's guidance [37]. In this study, data recording was performed for 40 min during each test to ensure data consistency and reliability. Testing was conducted three times to guarantee data reliability and consistency.

2.5. Experimental performance analysis

The vapor-compression refrigeration cycle is the chosen cycle for air-conditioning systems, featuring an isentropic compression process in the compressor [46]. Adiabatic processes entail no heat transfer between the fluid and its surroundings and vice versa. A reversible process occurs when the fluid remains in constant equilibrium, akin to a frictionless process in the compressor [47]. The isentropic process condition is both reversible and adiabatic. The saturation cycle, featuring isentropic compression in the RAC system, is illustrated in Fig. 5.

Performance analysis is the stage where each critical component of the refrigeration cycle is identified and evaluated. The performance of this analysis includes estimating the amount of refrigerant effect or heat absorbed by the evaporator, calculating compressor work, and evaluating the coefficient of performance [48]. The outcome of this analysis determines the overall coefficient of performance (COP) value for the RAC system. The vapor compression refrigeration cycle is expected to exhibit a no-pressure drop phenomenon in the condenser, evaporator, and all refrigerant lines in the RAC system test setup. The pressure gauge then indicates the condensing and evaporating pressures, which are expected to be equivalent to the discharge and suction pressures. Furthermore, any increases in kinetic and potential energy are considered to be insignificant. Temperature and pressure at a specific location play a critical role in influencing the RAC system's heat absorption, compressor effort, and COP. Enthalpy is calculated by considering both temperature and pressure simultaneously.

The following calculations of mass and energy balance are adopted to analyze the performance of the RAC system, as suggested by

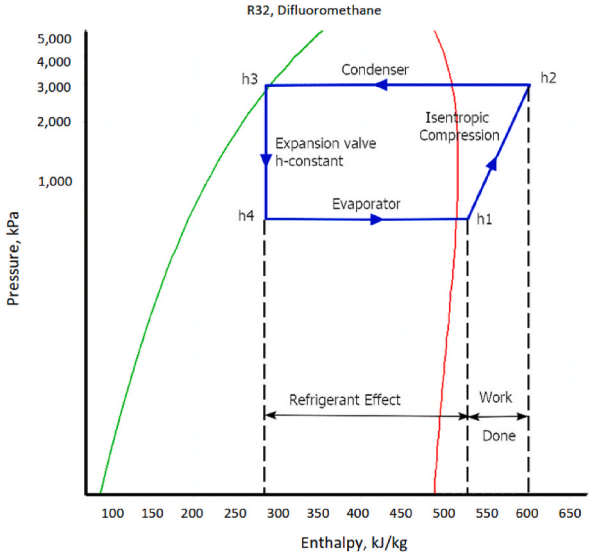

Fig. 5. Saturation cycle with isentropic compression.

previous researchers [18,47,49,50].

Heat absorbs or refrigerant effect (kJ/kg) [51].

$$Q_e = h_1 - h_4 \tag{2}$$

Compressor work done (kJ/kg) [51].

$$W_c = h_2 - h_1 \tag{3}$$

Cooling capacity or refrigerant duty (kW) [51].

$$Qe = m.(h_1 - h_4) \tag{4}$$

Refrigerant mass flow rate (kg/s) [51].

$$\dot{m} = \frac{Q_e}{(h_1 - h_4)} \tag{5}$$

According to the performance of each parameter of the RAC system, the overall COP can be determined by calculating the ratio between the refrigerant effect and the compressor work done, as expressed in equation (6).

$$COP = \frac{Q_e}{W_D} \tag{6}$$

Equation (6) is used to determine the compressor's electrical power [52].

$$P = V.I \tag{7}$$

2.6. Uncertainty and consistency analysis

This study employed a wide range of sensors and measurement tools. Performing a consistency analysis using the percent relative standard error (RSE) as suggested by a previous researcher, the measurement consistency and standard error that occurred in each of the mentioned parameters were evaluated [51]. Additionally, based on the % relative standard error (RSE) given by Yusri et al. [53], the measurement error of data collection for all performance metrics was computed. A consistency study, following Yusri et al. [53], was conducted to ensure the reliability and repeatability of the experimental data [53].

$$RSE = \frac{S_{eer}}{\overline{X}}\ x\ 100 \text{ where the standard error } S_{eer} \text{ using } S_{eer} = \frac{\sigma}{\sqrt{n}} \tag{8}$$

Where $\overline{X}$ is the mean, σ is the standard deviation, and n is the number of samples.

2.7. Response surface methodology optimization

The current study utilized the Central Composite Design (CCD) of the Response Surface Methodology (RSM) to identify the optimal operating conditions for the nanolubricant. Two parameters, specifically the volume concentration and initial refrigerant mass, were identified and employed to assess the RAC system's overall performance response, particularly the COP, for each type of nanolubricant paired with refrigerants R410a and R32. The data collection process was repeated three times for each nanolubricant concentration during the experiment. This step aimed to ensure data consistency, reliability, and the elimination of potential errors in data capture. This rigorous approach was undertaken before initiating the optimization calculation and analysis. While the minimum CCD center point is typically set to 5, this study increased it to 8 points to enhance the reliability of calculations and data processing [54]. Determining alpha one as the face aims to accurately establish the value within the intended boundary [55]. For optimization purposes, it is recommended that RSM perform 16 rounds of experimental analysis for each nanolubricant based on the CCD settings.

3. Results and discussion

Prior to conducting experiments, all equipment and apparatus used in this investigation underwent verification. The validation method for equipment and instruments was implemented in this study to ensure that measurement and data capture results during the experimental process are accurate, consistent, reliable, and free of errors. The experiments and data collection were subsequently repeated three times. This repetition was carried out to prevent data-gathering errors and ensure data reliability before proceeding to the data analysis procedure.

3.1. FAl_2O_3 nanoparticles characterization

The novel FAl_2O_3 nanoparticles were characterized using FEI Tecnai G2 T20 X-TWIN to determine their morphology, shape, and size. Fig. 6 depicts the results of the characterization of FAl_2O_3 suspended in POE. The TEM micrograph displays two dominant colors: dark and contrast-based. The intensity of the beam interacting with the sample and the thickness of the nanoparticles contribute to the

dark-to-black coloration.

Fig. 7 illustrates the distribution of novel FAl_2O_3 nanoparticle diameters. It is evident that the distribution follows a normal pattern based on Gaussian distribution analysis, with mean and standard deviation values. The graph is symmetrical, maintaining balance as it approaches the peak, with equal distances and patterns on both sides. No significant deviations are present on either the left or right side, nor are there valleys at the peak of the frequency distribution. The standard deviation indicates data variability or dispersion. A smaller standard deviation implies data points closer to the mean, resulting in a narrower peak. This demonstrates the reliability and homogeneity of the utilized FAl_2O_3 nanoparticles. According to the graph, the average diameter of the FAl_2O_3 nanoparticles is determined to be 43.11 nm.

The density of nanoparticles and the interaction between the characterizing nanoparticles simultaneously determine the thickness level. The micrograph confirms the dispersion of FAl2O3 in the POE, aligning with Liu's findings [56].

Fig. 8 displays the EDX evaluation results of FAl_2O_3 nanoparticles. It is evident that the displayed elements correspond to the elements constructing the nanoparticles. As shown in Fig. 8, the study involves interpreted FAl_2O_3 nanoparticles. The larger the EDX spectra peak, the greater the representation of the specific element, as summarized in Table 4.

3.2. FAl_2O_3-POE nanolubricant visual observation

On the first day, each nanolubricant sample exhibited extensive nanoparticle dispersion, with no signs of sedimentation in either type of nanolubricant. This observation suggests the excellent quality of dispersion in this nanolubricant sample. Ultrasonication treatment proves efficient in preventing aggregation and sedimentation of the nanolubricant sample. Observations continued on day 30; all samples remained highly stable, showing no significant signs of sedimentation. While there were hints of minor agglomeration, they were quite slight and primarily occurred in samples with higher concentrations, especially samples 4 and 5, as shown in Fig. 9. The minimal sedimentation in the nanolubricant sample highlights the strong repulsion between nanoparticle surfaces, minimizing the van der Waals attraction effect [57].

3.3. Heat absorbs and cooling performance evaluation

Figs. 10 and 11 illustrate the impact of the initial refrigerant charge on the heat absorption and cooling performance of FAl_2O_3–POE nanolubricants with R32 at various concentrations. The refrigerant charge in an air conditioning system is closely linked to the mass flow rate. The refrigerant charge denotes the quantity of refrigerant, usually measured in kilograms or pounds, in the system. In contrast, the mass flow rate indicates the mass of refrigerant passing through the system per unit of time, often measured in kilograms per second or pounds per minute. The refrigerant charge influences the mass flow rate by determining the amount of refrigerant present in the system to facilitate heat transfer and cooling. A proper refrigerant charge is crucial for the optimal operation of the air conditioning system.

When the refrigerant charge is too low, there isn't sufficient refrigerant to efficiently absorb heat from the indoor air. This situation can lead to diminished cooling capacity and poor performance, a finding consistent with prior researchers' earlier discoveries [58–60]. A low refrigerant charge can also result in the evaporator coil freezing due to insufficient heat absorption. Conversely, if the refrigerant charge is excessively high, it can also adversely affect the system's performance. An excessive amount of refrigerant can cause problems like heightened compressor workload, reduced heat transfer efficiency, and potential damage to system components, as reported by Porras et al. [61].

This event demonstrates a crucial aspect of the RAC system: the evaporator's capacity to absorb heat from the surrounding environment in 60 s [62]. In general, the FAl2O3–POE nanolubricant enhances heat absorption more than pure POE. According to the graph, heat absorption declines as the initial refrigerant charge decreases, which is directly related to the cooling capacity phenomenon. This phenomenon can be explained by an increase in the mass flow rate for each increment of refrigerant charge, resulting in

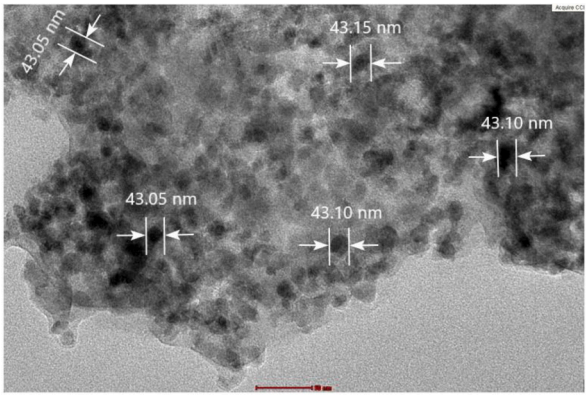

Fig. 6. TEM image of FAl_2O_3–POE Nanolubricant in 50.000 magnitude.

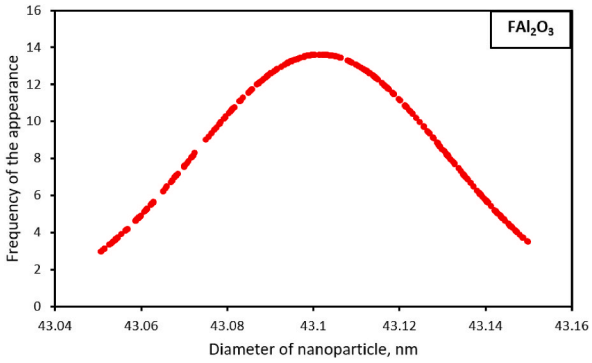

Fig. 7. Gaussian distribution of FAl_2O_3 Nanoparticles.

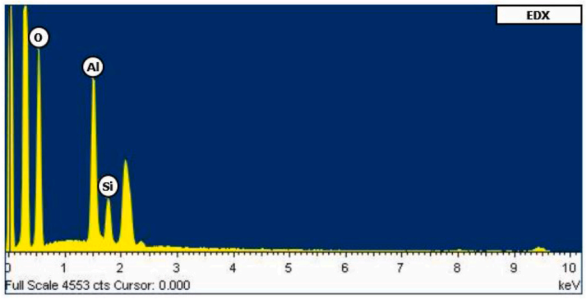

Fig. 8. EDX element analysis of FAl_2O_3 Nanoparticle.

Table 4
Element percentage of FAl_2O_3 nanoparticles.

Element	Weight %	Atomic %
Oxygen	64.17	75.34
Aluminum	25.78	17.95
Silicon	10.04	6.72
Total	100.00	–

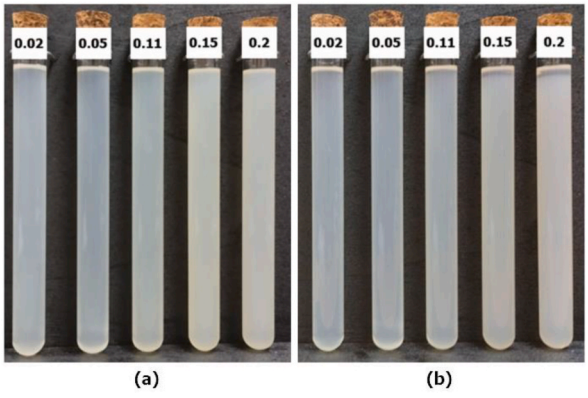

Fig. 9. Visual evaluation of FAl_2O_3-POE nanolubricant on (a) day 1 and (b) day 30.

higher refrigerant weight, which in turn affects the reduction in heat absorbed [63]. The cooling capacity exhibits the opposite phenomenon, with an improvement in cooling capacity performance as the initial refrigerant charge increases, as illustrated in Fig. 10.

The high refrigerant mass flow rate in the RAC system mixed with nanolubricant promotes higher nanoparticle collisions, enhancing cooling capacity compared to pure POE. Additionally, the wave movement generated by phonons of the dispersed

nanolubricant escalates the heat transfer in the system [64]. This cooling capacity improvement could be attributed to the enhancement in the higher refrigerant mass flow rate compared to the RAC system with pure POE lubricant. This situation directly influences the increased cooling capacity of the RAC system. However, the cooling capacity of the highest fraction of 0.2 vol% nanolubricant shows a decrement. This phenomenon can be explained by the fact that the density of the mixture of refrigerant and nanolubricant with 0.2 vol% increased tremendously, leading to an increase in the viscosity of the nanolubricant [65]. This condition has a direct impact on the lower mass flow rate. The cooling capacity of FAl2O3–POE/R3 increased by 5%–18%, respectively.

3.4. Compressor work evaluation

Fig. 12 illustrates the compressor performance phenomenon observed in the current investigation using FAl2O3–POE/R3. The graphs display the phenomenon of decreasing compressor work with increasing initial refrigerant charge. When the AAC system employs a limited amount of refrigerant, the compressor must exert greater effort to compress the refrigerant and raise system pressure. Consequently, the compressor's work is highest at the lowest initial refrigerant charge. Conversely, higher compressor work results in elevated inlet and outlet temperatures for the compressor at low initial refrigerant levels [17]. The utilization of nanolubricant can mitigate compressor work in the RAC system, leading to a decrease in compressor work due to the improved lubrication effect and tribological impact, as explained in the previous sub-section on tribology assessment. This phenomenon has a direct positive influence on the overall performance enhancement of the RAC system, as reported by Kamarulzaman [66].

The increase in compressor lubrication is linked to the tribological aspect, which transforms sliding motion into rolling motion [67]. This effect also influences the compressor's power input. However, there is a noticeable inclination for the compressor power input to rise as the initial refrigerant charge in the RAC system increases. This phenomenon is attributed to the impact of increasing the refrigerant mass flow rate for each initial refrigerant charge, which affects the compressor power input. This trend aligns with the findings reported by Adelekan et al. [11,68]. The experimental results demonstrated that the use of nanolubricant decreased compressor work by 4.91%–17.23%.

3.5. Coefficient of performance evaluation

Fig. 13 illustrates the coefficient of performance (COP) of FAl2O3–POE/R32 nanolubricants. The graphs generally indicate that increasing the initial refrigerant charge results in an increase in COP. Moreover, as the nanolubricant concentration increases, COP also rises. The COP shows a rise up to a concentration of 0.15 vol%, after which it decreases at a concentration of 0.2 vol%, approximately mirroring the increase in COP at a concentration of 0.02 vol%. This change in COP ranges from 3.12% to 32.26%. The most significant increase is observed at 0.15 vol%, with a COP improvement of 32.26% using an initial refrigerant charge of 0.442 kg.

The mechanism responsible for improving COP can be summarized as follows: COP increases as compressor work decreases [69]. This outcome stems from the reduction in compressor load, leading to a decrease in compressor work. This reduction in work is attributed to the tribological impact of nanolubricants, which can provide substantially better lubrication compared to pure POE lubricants. The introduction of nanolubricants has a significant positive effect on the COP value in the RAC system. This behavior is attributed to improvements in the compressor's heat transfer mechanism, cooling capacity, and overall energy efficiency. These findings align with the work of Ahmed and Elsaid et al. [49], which suggests that the use of nanolubricants can enhance the coefficient of performance in refrigeration systems. Similarly, Bakthavatchalam et al. [70] reported a substantial reduction in compressor work and a consequent increase in the coefficient of performance in air conditioning systems through the use of nanolubricants.

The decrease in COP for the nanolubricant with the highest concentration of 0.2 vol% is illustrated in Fig. 13. This phenomenon can be attributed to a significant increase in the density of the refrigerant and nanolubricant mixture under these conditions. The

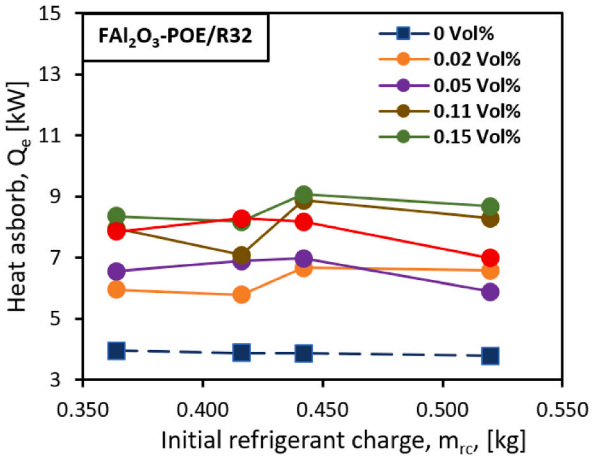

Fig. 10. Effect of initial refrigerant charge on heat absorption.

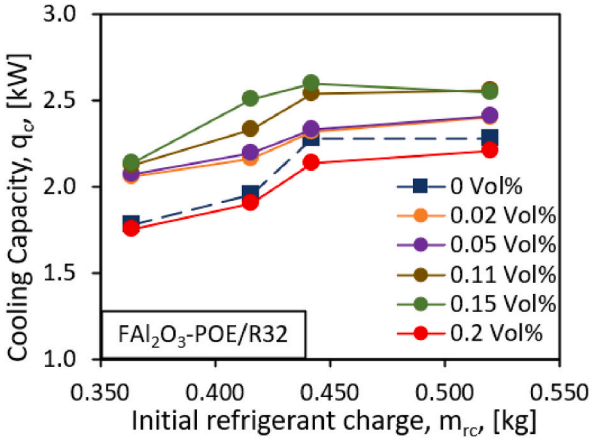

Fig. 11. Effect of initial refrigerant charge on the cooling capacity.

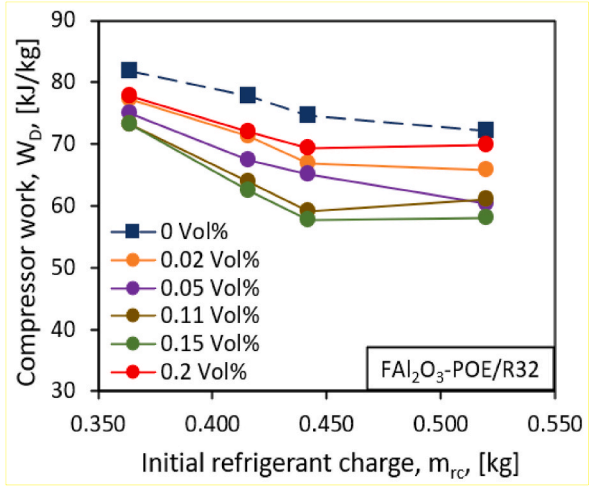

Fig. 12. Effect of initial refrigerant charge on compressor work.

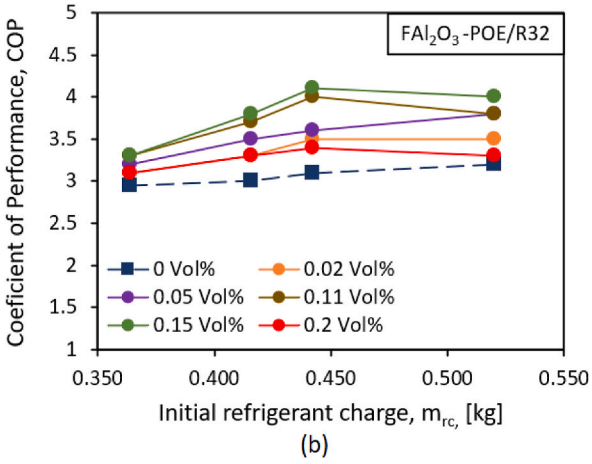

Fig. 13. COP RAC system in various initial refrigerant charge.

introduction of 0.2 vol% nanoparticles to the lubricant has a substantial impact on the viscosity of the nanolubricant. As a result, this phenomenon leads to a rise in pressure within the refrigerant line, consequently resulting in elevated temperatures at the inlet and outlet of the compressor. The substantial temperature increase at the discharge outlet of the compressor hampers the efficiency of the isentropic compression process, thereby leading to an increase in compressor work [71].

3.6. Power consumption evaluation

Fig. 14 illustrates the impact of nanolubricant utilization on the electrical power consumption of the RAC system. The graph demonstrates that the use of FAl_2O_3–POE nanolubricant results in decreased power consumption compared to pure POE lubricant. A decline in power consumption is evident at each concentration, up to 0.15 vol%. However, beyond this point, a substantial increase in power consumption surpasses the adoption of pure POE lubricant at the 0.2 vol%.

Therefore, the adoption of nanolubricant significantly decreases the electrical power demand of the RAC system's compressor. This reduction can be attributed to the influence of dispersed nanoparticles in the lubricant, which impacts the pressure drop at the suction and discharge inlets of the compressor. This pressure drop subsequently affects the low current entering the compressor, leading to a reduction in the required electrical power [72].

At a concentration of 0.2 vol%, there was an increase in the compressor's electrical current flow across all levels of the initial refrigerant charge and all types of nanolubricant. This phenomenon can be attributed to the higher concentration of nanoparticles (0.2 vol%), leading to elevated pressure levels in both the suction and discharge refrigerant lines [73]. Consequently, this rise in pressure contributed to an increase in temperature within the compressor's discharge line.

The escalation in operating pressure and temperature at a concentration of 0.2 vol% resulted in an augmentation of the current input to the RAC system. As a consequence, this situation prompted a rise in power consumption for the RAC system. However, the findings provide evidence that the application of FAl_2O_3–POE nanolubricant in conjunction with R32 leads to a reduction in electrical power consumption by 13.79%–19.35%, respectively.

3.7. Uncertainty and consistency analysis

Table 5 presents an overview of the outcomes from the RSE calculations. An authentic air conditioning system setup was employed in this investigation. The analysis of this study centered around critical parameters pertinent to the cooling system, including refrigerant effect or heat absorption, compressor work, cooling capacity, vibration displacement, and coefficient of performance (COP).

Consistency analysis was conducted in this study using Equation (8) to calculate the relative standard error (RSE), as recommended by previous researchers, in order to assess the measurement consistency and standard error of the mentioned parameters. In this study, RSE values were computed based on experimental data from three runs conducted under the same conditions.

3.8. Central composite design of response surface methodology outcome

The quadratic model is the exact model advocated for each RSM analysis. These models are determined by maximizing the modified R^2 and the projected R^2, as shown in Table 6.

3.8.1. ANOVA output

Table 7 demonstrates the analysis of variance for the quadratic model used to examine the adequacy of the FAl_2O_3-POE/R32 model developed by CCD RSM.

Table 7 presents the ANOVA response for FAl2O3–POE/R32. The table demonstrates that the ANOVA analysis yields a polynomial model with a p-value <0.0001, signifying the model's significance in fitting the experimental results within a 95% confidence level [74]. B, A^2, and B^2 are significant model terms in this context [75]. The model's F-value of 133.08 suggests its significance. The strong positive relationship between the analyzed factors and response is evident from the R^2 value of 0.9852. The predicted R^2 of 0.8933 reasonably aligns with the Adjusted R^2 of 0.9778. Adequate precision, which measures the signal-to-noise ratio [76], is represented by a ratio of 29.6774 in this model, indicating a sufficient signal. This finding is in line with the research by Fazeli et al. [77].

3.8.2. 2D contour and 3D surface plot analysis

Fig. 15 and Fig. 16. illustrate the correlation and interaction of factors in the optimization process of the present study, presented in 2D contour and 3D surface shapes, respectively. Utilizing the CCD RSM model, these plots were constructed to showcase the impact of factor variables and their interactions. Color variation indicates the effect of factor interaction. The curved and nearly round or oval shape of the 2D contour plots signifies the relevant characteristics of RSM optimization [78].

The 3D surface contour exhibits the optimal operating conditions within a red, dome-shaped zone. This prominent dome shape signifies the success of the optimization process. Consequently, the contour's red zone indicates the ideal operational parameters. The circular orbits observed in the 2D contour remain consistent across all regions of color variation, with no individual circular orbit deviating or appearing anomalous [79]. Each element examined demonstrates a noteworthy influence on the targeted response. This validation is evident on each matrix within Fig. 16 as a 3D surface.

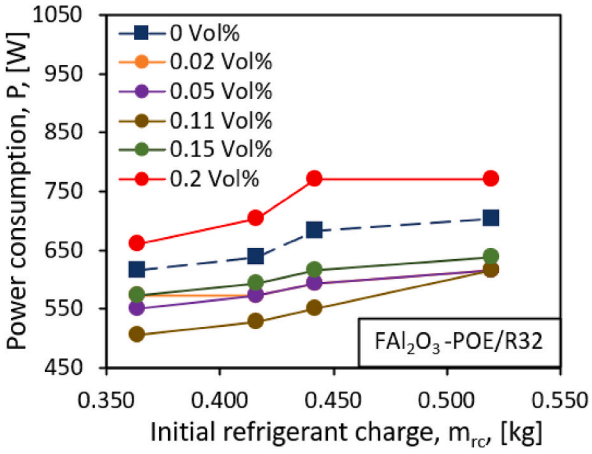

Fig. 14. Power consumption of RAC system in various initial refrigerant charge.

Table 5
Consistency values of the present study.

m_{rc} kg	Q_e [kJ/kg]	W_c [kJ/kg]	q_c [kW]	COP
0.364	0.05	0.04	0.05	0.04
0.416	0.04	0.05	0.04	0.03
0.442	0.03	0.04	0.05	0.05
0.520	0.03	0.04	0.05	0.03

Table 6
Model summary statistics FAl_2O_3-POE/R32.

Source	Std. Dev.	R^2	Adjusted R^2	Predicted R^2	PRESS	
Linear	0.3882	0.1355	0.0025	−0.6854	0.3882	
2FI	0.8050	0.1400	−0.0750	−2.8320	0.8050	
Quadratic	<0.0001	0.9852	0.9778	0.8933	<0.0001	Suggested
Cubic	0.6480	0.9867	0.9751	−0.4627	0.6480	Aliased

Table 7
ANOVA output of COP in FAl_2O_3-POE/R32.

Source	Sum of Squares	df	Mean Square	F-value	p-value	
Model	2.16	5	0.4315	133.08	<0.0001	significant
A-Volume Concentration	0.0150	1	0.0150	4.63	0.0570	
B-Refrigerant Charge	0.2817	1	0.2817	86.87	<0.0001	
AB	0.0100	1	0.0100	3.08	0.1096	
A^2	0.6182	1	0.6182	190.67	<0.0001	
B^2	0.3782	1	0.3782	116.65	<0.0001	
Residual	0.0324	10	0.0032			
Lack of Fit	0.0324	3	0.0108			
Pure Error	0.0000	7	0.0000			
Cor Total	2.19	15				
R^2	0.9852		Std. Dev.	0.0717		
Adjusted R^2	0.9778		Mean	3.55		
Predicted R^2	0.8933		C.V. %	2.02		
Adequate Precision	29.6774					

3.8.3. Optimization output

Table 8 presents the optimal solutions for each nanolubricant in the current evaluation. These solutions result from the determination of optimization criteria, which aims to achieve the "in range" COP value within the initial refrigerant charge range of 0.364%–0.52% and the concentration range of 0.02 vol% to 0.2 vol%. Subsequently, the standard error was chosen to be minimized. The RSM's desirability function is employed to identify the optimal operating condition. The desirability value ranges from 0 to 1, with 1

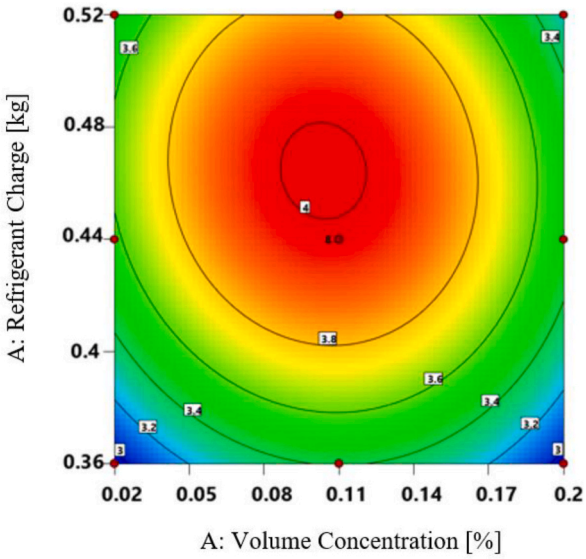

Fig. 15. Plot of FAl_2O_3–POE/R32 in 2D contour.

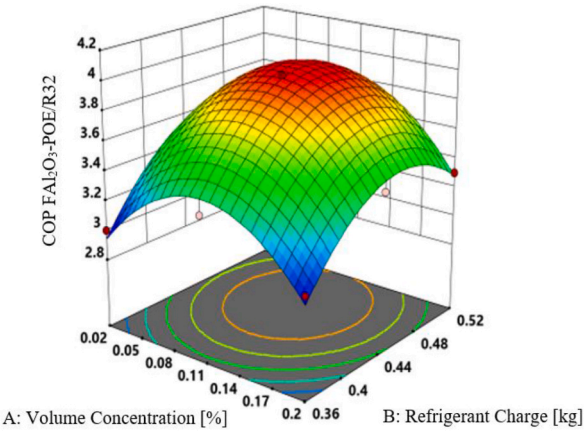

Fig. 16. Plot FAl_2O_3–POE/R32 in 3D surface.

representing the most favorable condition [80–82].

The graph illustrates the values of factors such as volume concentration and initial refrigerant charge, which serve as the operating conditions for the RAC system to attain the optimal COP. The optimal operating conditions are determined by considering the volume concentration, initial refrigerant charge, and COP within the "in range" parameters. These factors contribute to deriving the optimal solution using the developed model and its correlation, as shown in Fig. 17. This criterion was controlled by specifying the minimum standard error to ensure the acceptability of the RSM results and recommendations [83]. An important insight is that the optimal condition does not necessarily equate to the highest COP. Instead, the optimal condition revolves around the interaction relationship between the independent variables (concentration and initial refrigerant charge) and the dependent variable (COP). Consequently, while achieving the maximum COP is realized when applying FAl_2O_3–POE nanolubricant at a concentration of 0.15 vol% with an initial refrigerant charge of 0.442 kg, this scenario is not considered the optimum. The CCD-RSM suggests that the optimal condition is a concentration of 0.11 vol% with an initial refrigerant charge of 0.442 kg as depicted in Fig. 17(a). This selection is rational, given that adding nanoparticles at concentrations exceeding 0.11 vol% becomes ineffective for the RAC system.

Table 8
The optimized nanolubricant solution.

Nanolubricant	Volume Concentration (%)	Refrigerant Charge (kg)	COP	Std Error	Desirability
FAl_2O_3-POE/R32	0.110	0.442	3.982	0.019	1.000

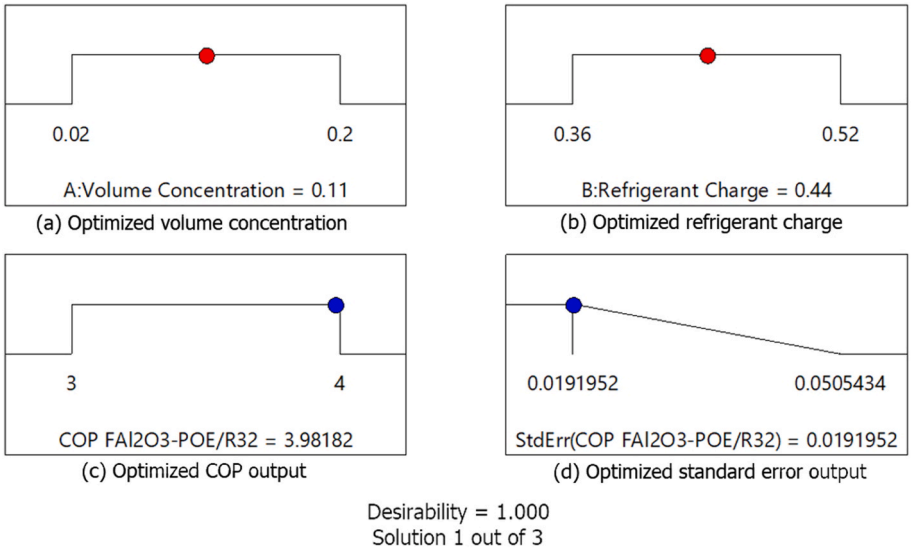

Fig. 17. Ramps diagram optimization solution for FAl_2O_3–POE/R32.

3.8.4. Optimization verification

The verification results of the RSM CCD optimization are shown in Table 9. The optimization analysis can be validated with a 95% confidence level. The standard variation between experimental results and forecasts is within 1%.

4. Conclusions

The evaluation yields several significant findings: Firstly, the utilization of nanolubricant in the RAC system enhances heat absorption; however, this absorption diminishes as the initial refrigerant charge decreases. Furthermore, increasing the initial refrigerant charge leads to improved cooling capacity performance. Secondly, the compressor work decreases up to a concentration of 0.15 vol% and then increases at 0.2 vol%. These findings shed light on the impact of nanolubricant utilization on heat absorption, cooling capacity performance, and compressor work at varying concentrations within the RAC system.

Thirdly, the incorporation of the novel FAl_2O_3–POE nanolubricant led to a rise in COP up to 0.15 vol%, followed by a decline at 0.2 vol%. The observed COP increase ranged from 3.12% to 32.26%, with the highest boost recorded at 0.15 vol% and an initial refrigerant charge of 0.442 kg. Electric power consumption decreased at all concentrations up to 0.15 vol%, but a noticeable surge in COP was seen at 0.2 vol%. The connection between initial refrigerant charge, nanolubricant concentration, and COP was affirmed by the high R2 value of 0.9852, supported by the ANOVA output (p-value <0.0001, F-value $= 133.08$). The optimal nanolubricant combination was identified at a concentration of 0.11% and an initial refrigerant charge of 0.442 kg, yielding a COP of 3.982 (standard error $=$ 0.019, desirability $= 1.000$).

In our investigation of air-cooled air conditioner performance testing, we have gained valuable insights into these cooling systems' capacity and efficiency ratings under various conditions. Our efforts have highlighted the factors influencing their operational effectiveness, helping us understand their behavior and potential improvements. The present investigation has illuminated essential aspects of air-cooled air conditioner performance testing. However, the absence of an ISO 5151:2017-certified experimental setup presents a limitation that signals an exciting pathway for future research. By aligning our methodology with this internationally recognized standard, we can enhance the rigor and reliability of our findings, ultimately contributing to a better understanding of air conditioning system capabilities and efficiencies. As researchers and practitioners, we encourage the integration of standardized protocols into performance testing endeavors, fostering a more cohesive and insightful body of knowledge in the field.

Table 9
Optimization validation of response surface methodology.

Parameter	Value
COP Predicted Mean	3.99933
COP Predicted Median	3.99933
COP Experimental Data	4
Std. Deviation	0.056942
Std. Error Prediction	0.060099
95% PI Low	3.86542
Mean	3.999325
95% PI High	4.13323

The significant rise in COP at a concentration of 0.11 vol% FAl2O3-POE presents a compelling pathway for extended exploration. The complex interplay between nanoparticle properties and lubricant behavior is likely the primary factor driving these enhanced performances. Investigating the altered physical properties of nanoparticles resulting from functionalization processes and their interactions with the base lubricant within the system unveils novel research prospects.

Author contribution statement

A. Nugroho: Conceived and designed the experiments; Performed the experiments; Analyzed and interpreted the data; Wrote the paper.

R. Mamat: Conceived and designed the experiments; Analyzed and interpreted the data; Contributed reagents, materials, analysis tools or data; Wrote the paper.

J. Xiaoxia, M. F. Jamlos, M. F. Ghazali: Analyzed and interpreted the data; Contributed reagents, materials, analysis tools or data; Wrote the paper.

Z. Bo: Conceived and designed the experiments; Contributed reagents, materials, analysis tools or data; Wrote the paper.

Data availability statement

Data included in article/supplementary material/referenced in article.

Declaration of competing interest

The authors declare that they have no known competing financial interests or personal relationships that could have appeared to influence the work reported in this paper.

Acknowledgments

The authors would like to extend their gratitude to Universiti Malaysia Pahang (UMP), Malaysia, for their generous financial support through the internal research fund RDU 190336 as well as to Ningxia University, China for their Helan Mountain research grant.

Nomenclature

FAl_2O_3	Functionalized Al_2O_3
min	Minute
vol %	Volume %
Std	Standard
POE	Polyolester
UV Vis	Ultra Violet visible
T	temperature(°C)
CCD	Central composite design
RSM	Response surface methodology
TEM	Transmission electron microscopy
COP	Coefficient of Performance
P	Power
V	Voltage
I	Current
h	Enthalpy

Greek symbols

φ	Volume concentration(%)
ρ	Density(kg/m^3)

Subscripts

L	Lubricant
P	Nanoparticle
c	Compressor
e	Evaporator

References

[1] C.I. Pardo Martínez, A. Cotte Poveda, Challenges and opportunities in the management of refrigeration and air conditioning systems to reduce environmental impacts in the Colombian health sector, Int. J. Refrig. 141 (2022) 54–65, https://doi.org/10.1016/j.ijrefrig.2022.06.002.

[2] R. di Filippo, O.S. Bursi, R. di Maggio, Global warming and ozone depletion potentials caused by emissions from HFC and CFC banks due to structural damage, Energy Build. 273 (2022), https://doi.org/10.1016/j.enbuild.2022.112385.

[3] W.Y. Park, N. Shah, E. Vine, P. Blake, B. Holuj, J.H. Kim, D.H. Kim, Ensuring the climate benefits of the Montreal Protocol: global governance architecture for cooling efficiency and alternative refrigerants, Energy Res. Social Sci. 76 (2021), https://doi.org/10.1016/j.erss.2021.102068.

[4] Y. Heredia-Aricapa, J.M. Belman-Flores, A. Mota-Babiloni, J. Serrano-Arellano, J.J. García-Pabón, Overview of low GWP mixtures for the replacement of HFC refrigerants: R134a, R404A and R410A, Int. J. Refrig. 111 (2020) 113–123, https://doi.org/10.1016/j.ijrefrig.2019.11.012.

[5] W.Y. Park, N. Shah, J.Y. Choi, H.J. Kang, D.H. Kim, A. Phadke, Lost in translation: overcoming divergent seasonal performance metrics to strengthen air conditioner energy-efficiency policies, Energy Sustain. Dev. 55 (2020) 56–68, https://doi.org/10.1016/j.esd.2020.01.003.

[6] S. Li, G. Wang, K. Zhang, X. Zhang, L. Zhang, W. Wang, R. He, Mechanical properties of Al2O3 and Al2O3/Al interpenetrated functional gradient structures by 3D printing and melt infiltration, J. Alloys Compd. 950 (2023), 169948, https://doi.org/10.1016/j.jallcom.2023.169948.

[7] X. Xie, D. Yang, Multi-functionalization of Al2O3 nanoparticles for enhancing thermal conductivity of epoxy natural rubber composites, Appl. Surf. Sci. 602 (2022), 154335, https://doi.org/10.1016/j.apsusc.2022.154335.

[8] W. Xu, P.C. Lemaire, K. Sharma, D.M. Hausmann, S. Agarwal, Extending growth inhibition during area-selective atomic layer deposition of Al2O3 on aminosilane-functionalized SiO2, Chem. Commun. 58 (2022) 6650–6652, https://doi.org/10.1039/d2cc01967a.

[9] I. Srivastava, A. Kotia, S.K. Ghosh, M.K.A. Ali, Recent advances of molecular dynamics simulations in nanotribology, J. Mol. Liq. 335 (2021), 116154, https://doi.org/10.1016/j.molliq.2021.116154.

[10] G.B.V. Kumar, R. Pramod, C.G. Sekhar, G.P. Kumar, T. Bhanumurthy, Investigation of physical, mechanical and tribological properties of Al6061–ZrO2 nano-composites, Heliyon 5 (2019), e02858, https://doi.org/10.1016/j.heliyon.2019.e02858.

[11] D.S. Adelekan, O.S. Ohunakin, M.H. Oladeinde, G. Jatinder, O.E. Atiba, M.O. Nkiko, A.A. Atayero, Performance of a domestic refrigerator in varying ambient temperatures, concentrations of TiO2 nanolubricants and R600a refrigerant charges, Heliyon 7 (2021), e06156, https://doi.org/10.1016/j.heliyon.2021.e06156.

[12] M. Hemmat Esfe, D. Toghraie, S. Alidoust, F. Amoozadkhalili, E. Mohammadnejad Ardeshiri, Investigating the rheological behavior of a hybrid nanofluid (HNF) to present to the industry, Heliyon 8 (2022), e11561, https://doi.org/10.1016/j.heliyon.2022.e11561.

[13] X. Cui, C. Li, M. Yang, M. Liu, T. Gao, X. Wang, Z. Said, S. Sharma, Y. Zhang, Enhanced grindability and mechanism in the magnetic traction nanolubricant grinding of Ti-6Al-4 V, Tribol. Int. 186 (2023), 108603, https://doi.org/10.1016/j.triboint.2023.108603.

[14] S.S. Sanukrishna, M. Jose Prakash, Experimental studies on thermal and rheological behaviour of TiO2-PAG nanolubricant for refrigeration system, Int. J. Refrig. 86 (2018) 356–372, https://doi.org/10.1016/j.ijrefrig.2017.11.014.

[15] X. Xu, Y. Hwang, R. Radermacher, Performance comparison of R410A and R32 in vapor injection cycles, Int. J. Refrig. 36 (2013) 892–903, https://doi.org/10.1016/j.ijrefrig.2012.12.010.

[16] V.H. Panato, D.F. Marcucci Pico, E.P. Bandarra Filho, Experimental evaluation of R32, R452B and R454B as alternative refrigerants for R410A in a refrigeration system, Int. J. Refrig. 135 (2022) 221–230, https://doi.org/10.1016/j.ijrefrig.2021.12.003.

[17] M.R. Salem, Performance enhancement of a vapor compression refrigeration system using R134a/MWCNT-oil mixture and liquid-suction heat exchanger equipped with twisted tape turbulator, Int. J. Refrig. 120 (2020) 357–369, https://doi.org/10.1016/j.ijrefrig.2020.09.009.

[18] D.F. Marcucci Pico, L.R.R. da Silva, P.S. Schneider, E.P. Bandarra Filho, Performance evaluation of diamond nanolubricants applied to a refrigeration system, Int. J. Refrig. 100 (2019) 104–112, https://doi.org/10.1016/j.ijrefrig.2018.12.009.

[19] G. Jatinder, O.S. Ohunakin, D.S. Adelekan, O.E. Atiba, A.B. Daniel, J. Singh, A.A. Atayero, Performance of a domestic refrigerator using selected hydrocarbon working fluids and TiO2–MO nanolubricant, Appl. Therm. Eng. 160 (2019), https://doi.org/10.1016/j.applthermaleng.2019.114004.

[20] N.F. Aljuwayhel, N. Ali, S.A. Ebrahim, A.M. Bahman, Experimental investigation of thermophysical properties, tribological properties and dispersion stability of nanodiamond-based nanolubricant for air conditioning systems, Int. J. Refrig. (2022), https://doi.org/10.1016/j.ijrefrig.2022.09.022.

[21] M.I. Ahmed, J.U. Ahamed, TiO2 nanolubricant: an approach for performance improvement in a domestic air conditioner, Results Mater 13 (2022), 100255, https://doi.org/10.1016/j.rinma.2022.100255.

[22] S.S. Chauhan, Performance evaluation of ice plant operating on R134a blended with varied concentration of Al2O3–SiO2/PAG composite nanolubricant by experimental approach 113 (2020) 196–205, https://doi.org/10.1016/j.ijrefrig.2020.01.021.

[23] A. Sigma, Al2O3 Certificate of Analysis, 2018.

[24] Z. Nugroho, Bo R. Mamat, W.H. Azmi, G. Najafi, F. Khoirunnisa, Extensive examination of sonication duration impact on stability of Al2O3-Polyol ester nanolubricant, Int. Commun. Heat Mass Tran. 126 (2021), 105418, https://doi.org/10.1016/j.icheatmasstransfer.2021.105418.

[25] N. Yuan, K. Tan, X. Zhang, A. Zhao, R. Guo, Synthesis and adsorption performance of ultra-low silica-to-alumina ratio and hierarchical porous ZSM-5 zeolites prepared from coal gasification fine slag, Chemosphere 303 (2022), 134839, https://doi.org/10.1016/j.chemosphere.2022.134839.

[26] G. Garbarino, T.K. Phung, G. Pampararo, P. Riani, G. Busca, Modification of the properties of γ-alumina as a support for nickel and molybdate catalysts by addition of silica, Catal. Today 378 (2021) 57–64, https://doi.org/10.1016/j.cattod.2021.02.016.

[27] R. Nugroho, Z. Mamat, Bo W.A, Hamzah Wan, M.F. Ghazali, T. Yusaf, Surface modification for dispersion stability of novel FAl2O3-POE nanolubricant using functional SiO2, in: N.H. Johari, W.A. Wan Hamzah, M.F. Ghazali, H.D. Setiabudi, S. Kumarasamy (Eds.), Proc. 2nd Energy Secur. Chem. Eng. Congr., Springer Nature Singapore, Singapore, 2023, pp. 179–192.

[28] S. Aljabair, A.L. Ekaid, S.H. Ibrahim, I. Alesbe, Mixed convection in sinusoidal lid driven cavity with non-uniform temperature distribution on the wall utilizing nanofluid, Heliyon 7 (2021), e06907, https://doi.org/10.1016/j.heliyon.2021.e06907.

[29] W.H. Azmi, K.V. Sharma, R. Mamat, G. Najafi, M.S. Mohamad, The enhancement of effective thermal conductivity and effective dynamic viscosity of nanofluids - a review, Renew. Sustain. Energy Rev. 53 (2016), https://doi.org/10.1016/j.rser.2015.09.081.

[30] A. Nugroho, R. Mamat, Z. Bo, W.A. Wan Hamzah, T. Yusaf, M.F. Ghazali, F. Khoerunnisa, A comprehensive investigation of low proportion TiO2-POE nanolubricant stability for residential air conditioning system application, Proc. 2nd Energy Secur. Chem. Eng. Congr. (2023) 147–163, https://doi.org/10.1007/978-981-19-4425-3_15.

[31] C. Mellado, T. Figueroa, R. Baez, M. Meléndrez, K. Fernández, Effects of probe and bath ultrasonic treatments on graphene oxide structure, Mater. Today Chem. 13 (2019) 1–7, https://doi.org/10.1016/j.mtchem.2019.04.006.

[32] M.Z. Sharif, W.H. Azmi, N.N.M. Zawawi, M.F. Ghazali, Comparative air conditioning performance using SiO2 and Al2O3 nanolubricants operating with Hydrofluoroolefin-1234yf refrigerant, Appl. Therm. Eng. 205 (2022), https://doi.org/10.1016/j.applthermaleng.2022.118053.

[33] A. Nugroho, R. Mamat, Z. Bo, W.A. Wan Hamzah, M.F. Ghazali, T. Yusaf, Surface modification for dispersion stability of novel FAl2O3-POE nanolubricant using functional SiO2, in: N.H. Johari, W.A. Wan Hamzah, M.F. Ghazali, H.D. Setiabudi, S. Kumarasamy (Eds.), Proc. 2nd Energy Secur. Chem. Eng. Congr., Springer Nature Singapore, Singapore, 2023, pp. 179–192.

[34] H. Ramírez, J. Jiménez-Cabas, A. Bula, Experimental data for an air-conditioning system identification, Data Br 25 (2019), 104316, https://doi.org/10.1016/j.dib.2019.104316.

[35] N. Shah, W.Y. Park, C. Ding, Trends in best-in-class energy-efficient technologies for room air conditioners, Energy Rep. 7 (2021) 3162–3170, https://doi.org/10.1016/j.egyr.2021.05.016.

[36] W. Zhou, Z. Gan, A potential approach for reducing the R290 charge in air conditioners and heat pumps, Int. J. Refrig. 101 (2019) 47–55, https://doi.org/10.1016/j.ijrefrig.2019.02.030.

[37] ISO, International, Standard 5151 Non-ducted Air Conditioners and Heat Pumps - Testing and Rating for Performance, 2017.

[38] F. Koksal, E. Mutluay, O. Gencel, Characteristics of isolation mortars produced with expanded vermiculite and waste expanded polystyrene, Constr. Build. Mater. 236 (2020), https://doi.org/10.1016/j.conbuildmat.2019.117789.

[39] L.E. Reynoso, Á.B. Carrizo Romero, G.M. Viegas, G.A. San Juan, Characterization of an alternative thermal insulation material using recycled expanded polystyrene, Constr. Build. Mater. 301 (2021), https://doi.org/10.1016/j.conbuildmat.2021.124058.

[40] A. Andrade, A. Restrepo, J.E. %J E.R. Tibaquira, EER or Fcsp: a performance analysis of fixed and variable air conditioning at different, cooling thermal conditions 7 (2021) 537–545.

[41] J. Lim, M.S. Yoon, T. Al-Qahtani, Y.%J.E. Nam, Feasibility study on variable-speed air conditioner under hot climate based on real-scale experiment and energy simulation 12 (2019) 1489.

[42] T.M.I. Mahlia, H.H. Masjuki, I.A. Choudhury, R. %J I.J. of P. Saidur, E. Systems, Testing and rating non-ducted air conditioners in Malaysia, The applicability of ISO standard 5151 22 (2002) 80–84.

[43] M.E. Abdur Razzaq, J.U. Ahamed, Thermodynamic analysis of an air conditioner using R22/HC blend with TiO2/Mineral oil nanolubricant to retrofit R22/POE oil, Results Eng 8 (2020), https://doi.org/10.1016/j.rineng.2020.100166.

[44] S. Anitha, K. Loganathan, M. Pichumani, Approaches for modelling of industrial energy systems: correlation of heat transfer characteristics between magnetohydrodynamics hybrid nanofluids and performance analysis of industrial length-scale heat exchanger, J. Therm. Anal. Calorim. 144 (2021) 1783–1798, https://doi.org/10.1007/s10973-020-10072-8.

[45] P. Mishra, S. Soni, G. Maheshwari, Exergetic performance analysis of low GWP refrigerants as an alternative to R410A in split air conditioner, Mater. Today Proc. 63 (2022) 406–412, https://doi.org/10.1016/j.matpr.2022.03.343.

[46] F. Kreith, R.M. Manglik, Principles of Heat Transfer, Cengage learning, 2016.

[47] Y.A. Cengel, M.A. Boles, M. Kanoglu, Thermodynamics - an Engineering Approach, Ninth Edit, McGraw-Hill Education, New York, 2019.

[48] H. Sun, Z. Duan, X. Wang, D. Wang, C. Wu, A pressure-node based dynamic model for simulation and control of aircraft air-conditioning systems, Energy 263 (2023), 125910, https://doi.org/10.1016/j.energy.2022.125910.

[49] M. Salem Ahmed, A.M. Elsaid, Effect of hybrid and single nanofluids on the performance characteristics of chilled water air conditioning system, Appl. Therm. Eng. 163 (2019), https://doi.org/10.1016/j.applthermaleng.2019.114398.

[50] V. Nair, A.D. Parekh, P.R. Tailor, Experimental investigation of a vapour compression refrigeration system using R134a/Nano-oil mixture, Int. J. Refrig. 112 (2020) 21–36, https://doi.org/10.1016/j.ijrefrig.2019.12.009.

[51] R.W. James, T.C. Welch, Chapter 9 - refrigeration and heat-pump systems, in: R. Legg (Ed.), Air Cond. Syst. Des., Butterworth-Heinemann, 2017, pp. 167–189, https://doi.org/10.1016/B978-0-08-101123-2.00009-1.

[52] A. Zankat, K. Gadani, B. Rajyaguru, K. Sagapariya, V. Pachchigar, M. Ranjan, K. Asokan, P.S. Solanki, N.A. Shah, D.D. Pandya, Current–voltage characteristics of manganite based p–n interfaces: role of swift heavy ion irradiation and defect annihilation, Phys. B Condens. Matter 614 (2021), 413013, https://doi.org/10.1016/j.physb.2021.413013.

[53] I.M. Yusri, R. Mamat, G. Najafi, A. Razman, O.I. Awad, W.H. Azmi, W.F.W. Ishak, A.I.M. Shaiful, Alcohol based automotive fuels from first four alcohol family in compression and spark ignition engine: a review on engine performance and exhaust emissions, Renew. Sustain. Energy Rev. 77 (2017) 169–181, https://doi.org/10.1016/j.rser.2017.03.080.

[54] M. Leili, N. Shirmohammadi Khorram, K. Godini, G. Azarian, R. Moussavi, A. Peykhoshian, Application of central composite design (CCD) for optimization of cephalexin antibiotic removal using electro-oxidation process, J. Mol. Liq. 313 (2020), 113556, https://doi.org/10.1016/j.molliq.2020.113556.

[55] A. Dejean, I.W.K. Ouédraogo, S. Mouras, J. Valette, J. Blin, Shea nut shell based catalysts for the production of ethanolic biodiesel, Energy Sustain. Dev. 40 (2017) 103–111, https://doi.org/10.1016/j.esd.2017.07.006.

[56] B. Liu, S. Yu, Y. Wang, H.Cong Shen, Preparation, surface functionalization and application of Fe3O4 magnetic nanoparticles, Adv. Colloid Interface Sci. 281 (2020), 102165, https://doi.org/10.1016/j.cis.2020.102165.

[57] P. Tiam, C. Gervais, N. Ketchate, D. Fokwa, G. Tchuen, Linear stability analysis of (Cu-Al2O3)/water hybrid nanofluid flow in porous media in presence of hydromagnetic, small suction and injection effects, Alexandria Eng. J. 60 (2021) 1525–1536, https://doi.org/10.1016/j.aej.2020.11.007.

[58] H.Y. Tsai, C.T. Wu, Optimization of a rotary desiccant wheel for enthalpy recovery of air-conditioning in a humid hospitality environment, Heliyon 8 (2022), e10796, https://doi.org/10.1016/j.heliyon.2022.e10796.

[59] G. Swamy, Development of an indoor air purification system to improve ventilation and air quality, Heliyon 7 (2021), e08153, https://doi.org/10.1016/j.heliyon.2021.e08153.

[60] H. Ramirez-Leon, M.A. Gonzalez-Carmona, J. Jimenez-Cabas, J. Escorcia-Gutierrez, A. Bula, Experimental air conditioning energy evaluation under Caribbean climate conditions, Heliyon 9 (2023), e14464, https://doi.org/10.1016/j.heliyon.2023.e14464.

[61] F. Porras, A. Walter, G. Soriano, A.D. Ramirez, On the adoption of stricter energy efficiency standards for residential air conditioners: case study Guayaquil, Ecuador, Heliyon 9 (2023), e13893, https://doi.org/10.1016/j.heliyon.2023.e13893.

[62] S. Vashisht, D. Rakshit, Recent advances and sustainable solutions in automobile air conditioning systems, J. Clean. Prod. 329 (2021), 129754, https://doi.org/10.1016/j.jclepro.2021.129754.

[63] M. Deymi-Dashtebayaz, M. Farahnak, M. Moraffa, A. Ghalami, N. Mohammadi, Experimental evaluation of refrigerant mass charge and ambient air temperature effects on performance of air-conditioning systems, Heat Mass Transf 54 (2017) 803–812, https://doi.org/10.1007/s00231-017-2173-6.

[64] S. Mazumder, Boltzmann transport equation based modelling of phonon heat conduction: progress and challenges, Annu. Rev. Heat Transf. 24 (2022).

[65] R. Kedzierski, K.T. Brignoli, J.S. Quine, Brown, Viscosity, density, and thermal conductivity of aluminum oxide and zinc oxide nanolubricants M.A, Int. J. Refrig. 74 (2017) 1–9, https://doi.org/10.1016/j.ijrefrig.2016.10.003.

[66] K.M. Kamarulzaman, S. Hisham, K. Kadirgama, D. Ramasamy, M. Samykano, R. Saidur, T. Yusaf, Improving the thermophysical properties of hybrid nanocellulose-copper (II) oxide (CNC-CuO) as a lubricant additives: a novel nanolubricant for tribology application, Fuel 332 (2023), 126229, https://doi.org/10.1016/j.fuel.2022.126229.

[67] S.K. Joysula, A. Dube, D. Patro, D.H. Veeregowda, On the fictitious grease lubrication performance in a four-ball tester, Lubricants 9 (2021), https://doi.org/10.3390/lubricants9030033.

[68] D.S. Adelekan, O.S. Ohunakin, J. Gill, O.E. Atiba, I.P. Okokpujie, A.A. Atayero, I.P. Okokpujie, Performance of a domestic refrigerator infused with safe charge performance of a domestic refrigerator infused with safe charge of R600a refrigerant and various concentrations of TiO2 of R600a refrigerant and various concentrations of TiO2 nanolubricants, Procedia Manuf. 35 (2019) 1158–1164, https://doi.org/10.1016/j.promfg.2019.06.071.

[69] T.O. Babarinde, S.A. Akinlabi, D.M. Madyira, F.M. Ekundayo, P.A. Adedeji, Dataset and ANN model prediction of performance of graphene nanolubricant with R600a in domestic refrigerator system, Data Br 32 (2020), 106098, https://doi.org/10.1016/j.dib.2020.106098.

[70] B. Bakthavatchalam, K. Habib, R. Saidur, B.B. Saha, Cooling performance analysis of nanofluid assisted novel photovoltaic thermoelectric air conditioner for energy efficient buildings, Appl. Therm. Eng. 213 (2022), 118691, https://doi.org/10.1016/j.applthermaleng.2022.118691.

[71] M. Yang, B. Wang, X. Li, W. Shi, L. Zhang, Evaluation of two-phase suction, liquid injection and two-phase injection for decreasing the discharge temperature of the R32 scroll compressor, Int. J. Refrig. 59 (2015) 269–280, https://doi.org/10.1016/j.ijrefrig.2015.08.004.

[72] C. Liang, Y. Wang, X. Li, Energy-efficient air conditioning system using a three-fluid heat exchanger for simultaneous temperature and humidity control, Energy Convers. Manag. 270 (2022), 116236, https://doi.org/10.1016/j.enconman.2022.116236.

[73] M. Salem Ahmed, M.R.A. Hady, G. Abdallah, Experimental investigation on the performance of chilled-water air conditioning unit using alumina nanofluids, Therm. Sci. Eng. Prog. 5 (2018) 589–596, https://doi.org/10.1016/j.tsep.2017.07.002.

[74] R. Aabeyir, S. Adu-Bredu, W.A. Agyare, M.J.C. Weir, Empirical evidence of the impact of commercial charcoal production on Woodland in the Forest-Savannah transition zone, Ghana, Energy Sustain. Dev. 33 (2016) 84–95, https://doi.org/10.1016/j.esd.2016.03.005.

[75] C. Camposeco-Negrete, Optimization of cutting parameters using Response Surface Method for minimizing energy consumption and maximizing cutting quality in turning of AISI 6061 T6 aluminum, J. Clean. Prod. 91 (2015) 109–117, https://doi.org/10.1016/j.jclepro.2014.12.017.

[76] L.T. Dufera, W. Hofacker, A. Esper, O. Hensel, Experimental evaluation of drying kinetics of tomato (Lycopersicum Esculentum L.) slices in twin layer solar tunnel dryer, Energy Sustain. Dev. 61 (2021) 241–250, https://doi.org/10.1016/j.esd.2021.03.003.
[77] I. Fazeli, M.R. Sarmasti Emami, A. Rashidi, Investigation and optimization of the behavior of heat transfer and flow of MWCNT-CuO hybrid nanofluid in a brazed plate heat exchanger using response surface methodology, Int. Commun. Heat Mass Tran. 122 (2021), 105175, https://doi.org/10.1016/j.icheatmasstransfer.2021.105175.
[78] M. Yuan, H. Feng, W. Zhang, J. Zheng, K. Zhang, X. Kong, N. Han, J. Dong, Gas-liquid sulfonation in T-shaped microchannel for DBSA synthesis and process optimization with response surface method, Chem. Eng. Process. - Process Intensif. 174 (2022), https://doi.org/10.1016/j.cep.2022.108890.
[79] M.S. Ashraf, M.U. Hassan Shah, A. Bokhari, M. Hasan, Less is more: optimising the biocementation of coastal sands by reducing influent urea through response surface method, J. Clean. Prod. 315 (2021), https://doi.org/10.1016/j.jclepro.2021.128208.
[80] M. Hemmat Esfe, S. Alidoust, E. Mohammadnejad Ardeshiri, D. Toghraie, Comparative rheological study on hybrid nanofluids with the same structure of MWCNT (50%)-ZnO(50%)/SAE XWX to select the best performance of nano-lubricants using response surface modeling, Colloids Surfaces A Physicochem. Eng. Asp. 641 (2022), https://doi.org/10.1016/j.colsurfa.2022.128543.
[81] M. Hemmat Esfe, S.M. Motallebi, D. Toghraie, Optimal viscosity modelling of 10W40 oil-based MWCNT (40%)-TiO(2) (60%) nanofluid using Response Surface Methodology (RSM), Heliyon 8 (2022), e11944, https://doi.org/10.1016/j.heliyon.2022.e11944.
[82] B. Sadhukhan, N.K. Mondal, S. Chattoraj, Optimisation using central composite design (CCD) and the desirability function for sorption of methylene blue from aqueous solution onto Lemna major, Karbala Int. J. Mod. Sci. 2 (2016) 145–155, https://doi.org/10.1016/j.kijoms.2016.03.005.
[83] X. Wei, X. Qiao, T. Chen, Design framework for rehabilitation grout materials during metro operation period: a combination of improved central composite design modeling and multi-objective particle swarm optimization, Constr. Build. Mater. 401 (2023), 132690, https://doi.org/10.1016/j.conbuildmat.2023.132690.